

Anderson localisation of Ion-Temperature-Gradient Modes and Ion Temperature Clamping in Aperiodic Stellarators

Amitava Bhattacharjee¹

¹Department of Astrophysical Sciences, Princeton University Correspondence: amitava@princeton.edu

Abstract

Ion temperature clamping — the saturation of the ion temperature regardless of heating power — is observed across stellarator experiments. We propose a minimal model based on Anderson localisation. Starting from a reduced fluid model for drift waves [*Phys. Fluids* **26**, 880 (1983)], we show that aperiodic stellarator geometry leads to a quasiperiodic Hill equation for the ion-temperature-gradient (ITG) mode structure. In a tight-binding approximation this equation reduces to an Aubry–Andre–Harper difference equation, suggesting an Anderson-localisation mechanism for ITG eigenfunctions. We identify a three-threshold ordering: the linear instability threshold lies below the Anderson localisation threshold, which lies below the observed clamp. This is conjectured to create a low-transport second regime above the instability threshold, qualitatively analogous to the second stability regime of MHD ballooning theory, and provides a power-independent lower bound on the observed gradient.

1. Introduction

A persistent feature of stellarator experiments is the saturation of ion temperature despite increasing heating power. In Wendelstein 7-X (W7-X) [1, 2] and the Large Helical Device (LHD) [3] the ion temperature T_i typically remains fixed, even when the applied heating power is increased substantially and the electron temperature T_e increases over a wide range. This phenomenon is commonly referred to as *ion-temperature clamping*. Measurements show that the ion-temperature-gradient (ITG) drive parameter, η_i , remains nearly constant over a wide range of heating powers. In contrast, standard quasilinear ITG transport theory predicts that the ion temperature increases linearly with heating power [4, 5], directly contradicting this observation.

The key experimental signature is that it is the *gradient*, not just the temperature level, that saturates. Dedicated power scans show that $\eta_i = L_n/L_{T_i}$, which is the dimensionless ratio of the logarithmic density gradient to the logarithmic ITG scale lengths, is generally locked near a value significantly above the linear instability threshold throughout the confinement region, with T_i adjusting to maintain this gradient rather than responding to deposited power [6]. Profile stiffness — the sharp increase of turbulent transport above the *linear* threshold η_i^{lin} — would pin the gradient near η_i^{lin} , not at the observed value η_i^{obs} , which is usually larger than η_i^{lin} . The observed saturation is therefore not explained by profile stiffness alone: a second, higher threshold must exist at which transport is suppressed and the gradient can stabilize.

In this work we propose that an important clamping mechanism in stellarators arises from the Anderson localisation [7] of ITG eigenmodes caused by the three-dimensional (3D) magnetic geometry. In the ballooning representation of the ITG instability, one obtains a differential equation along the magnetic field line whose coefficients depend on the magnetic curvature and drift frequencies. In stellarators these quantities

are not strictly periodic along a field line but instead vary aperiodically because the field line samples the full 3D geometry of the magnetic field. As a result, under some simplifying assumptions, the ITG eigenvalue problem becomes an *aperiodic Hill equation*. Differential operators of this type are closely related to the Aubry–André–Harper (AAH) model [8, 9]. Such operators are known to exhibit localisation transitions in which eigenfunctions change from spatially extended Bloch states to exponentially localized Anderson states as the amplitude of the aperiodic modulation increases. Such a phenomenon has been recently identified in the context of linear [10, 11] and nonlinear magnetohydrodynamic (MHD) stability [12] of ballooning modes in stellarators.

The key idea of the present paper is that a similar localisation transition can occur for ITG eigenmodes in stellarators. The discrete AAH limit has a sharp localisation transition with no mobility edge (in condensed matter physics parlance). The continuous quasiperiodic Hill equation considered here is AAH-like, but its threshold must be computed from the Lyapunov exponent at the relevant eigenvalue. We therefore use the onset of a positive Lyapunov exponent at the drift-wave-resonant energy as the localisation diagnostic for the reduced fluid model.

The localisation threshold η_i^* depends on the dimensionless magnetic drift and curvature profile along the field line and must be computed from the Lyapunov exponent, discussed below. The accurate threshold for any real 3D device requires the full Boozer harmonic spectrum for the background equilibrium, which is sensitive to geometry. The transition point η_i^* marks the boundary between a regime ($\eta_i^{\text{lin}} < \eta_i < \eta_i^*$) and an Anderson-localized regime ($\eta_i > \eta_i^*$) — the ITG analogue of the second stability regime in MHD ballooning theory. In the ballooning problem the suppression arises from linear restabilization, whereas here it is conjectured to arise from topological localisation of the eigenmodes.

The aim of the present work is not to construct a complete

transport model but rather to identify a structural property of the ITG eigenvalue problem in 3D magnetic geometry. If the proposed localisation mechanism is confirmed by simulation and experiment, it could establish a direct connection between stellarator magnetic geometry and Anderson localisation physics, providing a new perspective on turbulent transport in magnetically confined plasmas.

2. From the two-fluid ITG equation to the Aubry–André–Harper map

2.1. The two-fluid ITG equation and its Schrödinger form

In the long-wavelength fluid limit, with the ballooning representation [13] and a *straight stellarator* geometry, Bhat-tacharjee et al. [14] reduced the drift-wave eigenmode problem to a single Schrödinger-like equation for the normalized electrostatic potential $\phi \equiv e\tilde{\phi}/T_e$ along the field-line coordinate $\theta = k_0 s$ (where s is arc length along the field line and $k_0 = \omega_{*e}/c_s$ is the normalization wavenumber with ω_{*e} is the electron diamagnetic frequency, $c_s^2 \equiv T_e/m_i$, and m_i is the ion mass). Here we extend their treatment by including an ion-temperature gradient. The relevant two-fluid ITG equation is derived in Appendix A:

$$\frac{d^2\phi}{d\theta^2} + [\Omega(\Omega - 1) + \epsilon_d(\theta)(\Omega + \eta_i)]\phi = 0. \quad (1)$$

Here $\Omega \equiv \omega/\omega_{*e}$ is the normalized eigenfrequency, $\epsilon_d(\theta) = \epsilon_n K(\theta)$, $\epsilon_n = L_n/R$ is the ratio of density gradient scale length to major radius, $\eta_i = L_n/L_{T_i}$ is the dimensionless ratio of the logarithmic density gradient scale length to the logarithmic ion-temperature-gradient scale length. We define the quantity $\omega_d(\theta)$ as the combined magnetic curvature and gradient- B drift frequency, defined through the field-line variation of the magnetic field strength:

$$\omega_d(\theta) \equiv \omega_{*e} \epsilon_n K(\theta) = \omega_{*e} \epsilon_d(\theta) \quad (2)$$

Here the normalisation by ϵ_n ensures $|K| \sim 1$. We choose model forms for $K(\theta)$ to represent tokamaks and stellarators qualitatively in this paper.

We now consider the drift-wave-resonant branch

$$\Omega = 1 + \Lambda, \quad |\Lambda| \ll 1.$$

Then

$$\Omega(\Omega - 1) = \Lambda + O(\Lambda^2), \quad \Omega + \eta_i = 1 + \eta_i + O(\Lambda).$$

We then obtain the Hill equation

$$\frac{d^2\phi}{d\theta^2} + \epsilon_n(1 + \eta_i)K(\theta)\phi = -\Lambda\phi. \quad (3)$$

We emphasize that this reduced equation is a leading-order mode-structure equation. For real $K(\theta)$, it does not by itself determine the ITG growth rate. Growth rates and a quantitative critical gradient require the effects omitted here, including finite-Larmor-radius corrections, kinetic resonances, non-adiabatic ion response, and the full stellarator magnetic-drift geometry.

The normalisation $\Omega = \omega/\omega_{*e}$ and the entire framework that follows are valid only when the drift-wave frequency ω_{*e} is finite and non-zero, i.e. when the density gradient is finite ($L_n < \infty$, η_i well-defined). In the flat-density limit $L_n \rightarrow \infty$ (equivalently $a/L_n \rightarrow 0$, $\eta_i \rightarrow \infty$), the drift-wave frequency vanishes, and the ITG mode becomes a purely curvature-driven mode not described by Eq. (1). Gyrokinetic simulations performed at $a/L_n = 0$ (flat density, $\eta_i = \infty$) operate in this different regime and are not directly comparable to the results of this paper. For recent comprehensive numerical studies relevant to W7-X, see [15, 16].

2.2. Aperiodic stellarator geometry: a simple model

In an aperiodic stellarator the magnetic field strength along a field line cannot be written as a function of a single angle, because the field line samples the full 3D geometry. Writing the field-line-following field strength as

$$B(\theta) = B_0 [1 - B_1 \cos \theta - B_2 \cos(\alpha\theta + \delta) + \dots], \quad (4)$$

For the illustrative model used here, we approximate the magnetic drift function rather than the magnetic-field strength itself by a two-harmonic form,

$$K(\theta) = \cos \theta + \lambda \cos(\alpha\theta + \delta).$$

In a quantitative stellarator calculation, λ and α should be extracted from the Fourier spectrum of $\omega_d(\theta)$.

For a two-harmonic stellarator model, the reduced equation then becomes

$$\frac{d^2\phi}{d\theta^2} + \epsilon_n(1 + \eta_i) [\cos \theta + \lambda \cos(\alpha\theta + \delta)]\phi = -\Lambda\phi. \quad (5)$$

In the equivalent Schrödinger-like equation, the effective potential $V(\theta)$ in Eq. (5) is therefore

$$V(\theta) = -\epsilon_n(1 + \eta_i) [\cos \theta + \lambda \cos(\alpha\theta + \delta)], \quad (6)$$

and the energy eigenvalue is Λ .

The wavenumber α is not a free parameter but is determined by the magnetic geometry. In Boozer coordinates (θ_B, ϕ_B) the field-strength harmonic $B_{m,n}$ varies as $\cos(m\theta_B - n\phi_B)$. Along a field line, θ_B and ϕ_B are related by $d\theta_B/d\phi_B = \iota$, the rotational transform, so $B_{m,n}$ contributes a term with field-line wavenumber

$$k_{m,n} = m - n/\iota. \quad (7)$$

The two dominant oscillatory harmonics of $B(\theta)$ along the field line have wavenumbers $k_1 = m_1 - n_1/\iota$ and $k_2 = m_2 - n_2/\iota$, so their ratio is

$$\alpha = \frac{k_2}{k_1} = \frac{m_2 - n_2/\iota}{m_1 - n_1/\iota}. \quad (8)$$

This is *irrational* whenever ι is irrational and the two modes are not in the same harmonic family ($m_1 n_2 \neq m_2 n_1$). Since the rational numbers form a set of Lebesgue measure zero on the real line, almost every flux surface carries an irrational

rotational transform, and rational surfaces ($\iota = p/q$, closed field lines) form a set of measure zero. The Kolmogorov–Arnold–Moser (KAM) theorem further guarantees that these irrational tori persist under small perturbations of an integrable magnetic field [17]. Incommensurability is therefore a generic property of stellarator field lines, not an additional assumption.

The introduction of the incommensurate term $\lambda \cos(\alpha\theta + \delta)$ is motivated at three distinct levels. *First*, it reflects physical reality: as shown in Eqs. (7)–(8), the wavenumber ratio α of the two dominant Boozer harmonics is determined by the rotational transform ι , and is irrational for almost all flux surfaces. The amplitude λ is a measurable equilibrium property, not a free parameter. Both α and λ can be extracted from an equilibrium reconstruction independently of any transport measurement. *Second*, it is what converts the Mathieu equation into the AAH model: the second incommensurate harmonic (with α irrational) destroys the band structure and replaces it with the sharp global transition at $\lambda = 1$ — it is precisely the irrationality of α that makes the transition sharp, since a rational α would merely produce a longer-period Mathieu equation with bands. *Third*, near marginal stability the single-harmonic Mathieu transition is a gradual crossover, not a sharp phase transition; the incommensurate perturbation present naturally in the stellarator equilibrium converts this crossover into the clean AAH transition.

2.3. The AAH exact result

The effective AAH coupling of the quasiperiodic component is

$$\lambda_{\text{AAH}} = \frac{A\lambda F_\alpha}{2|t|} = \frac{\epsilon_n(1 + \eta_i)\lambda F_\alpha}{2|t|}. \quad (9)$$

where t and F_α are the Wannier hopping and form factors defined in Appendix B.

Aubry and André [8] solved the map associated with Eq. (5) exactly. The result is:

- $|\lambda_{\text{AAH}}| < 1$: extended states in the discrete AAH model.
- $|\lambda_{\text{AAH}}| = 1$: the critical point.
- $|\lambda_{\text{AAH}}| > 1$: exponentially localized states, with

$$\xi_{\text{AAH}} = \frac{1}{\ln |\lambda_{\text{AAH}}|}. \quad (10)$$

where λ_{AAH} is the dimensionless coupling of the discrete tight-binding model (Appendix B).

The result (10) is exact for the *discrete* AAH model, requires no perturbation theory, and holds for all eigenstates simultaneously and for all irrational α (Fig. 1). It is one of the rare exactly solvable problems in the theory of disordered systems.

3. The localisation threshold

3.1. The Lyapunov exponent as the localisation criterion

The AAH exact result (Section 2.3) establishes the *topology* of the localisation transition: for irrational α , all eigenstates localize simultaneously at $\lambda_{\text{AAH}} = 1$, with no mobility edge.

For the *continuous* quasiperiodic Hill equation (3), the precise threshold must be computed from the equation itself, as done in [12] for ballooning modes. To do so, we write Eq. (3) as a first-order system and integrate it numerically along the field line. The fundamental quantity is the Lyapunov exponent. Let $T_N(\Lambda, \eta_i)$ be the transfer matrix that advances (ϕ, ϕ') from $\theta = 0$ to $\theta = 2\pi N$. The Lyapunov exponent per field-line period is

$$\gamma(\Lambda, \eta_i) = \lim_{N \rightarrow \infty} \frac{1}{N} \ln \|T_N(\Lambda, \eta_i)\|. \quad (11)$$

In numerical work this limit is evaluated by accumulating the logarithms of the norms after each period [18]. By the Oseledec's theorem [19], γ exists and is independent of the initial condition (for almost every initial condition). A positive Lyapunov exponent indicates exponential separation of solutions and the existence of exponentially decaying solutions when the corresponding energy lies in the spectrum. We therefore use the onset of $\gamma > 0$ at the drift-wave-resonant value $\Lambda = 0$ as the localisation diagnostic for the reduced model. For the discrete AAH model, $\gamma = \ln \lambda$ for $\lambda > 1$ [8], confirming the sharp simultaneous transition. The threshold η_i^* is the value of η_i at which γ first becomes positive. At $\Lambda = 0$, the hopping amplitude $\epsilon_n(1 + \eta_i)$ increases with η_i , driving the quasiperiodic potential deeper until the Lyapunov exponent turns on, and modes are Anderson-localised.

Numerical result. Figure 2 shows $\gamma(\eta_i)$ computed with $N = 200$ field-line periods for the model geometry ($\lambda = 1$, $\alpha = 2.1$, $\epsilon_n = 0.12$) and for the periodic device ($\lambda = 0$, same ϵ_n). The Lyapunov exponent is noisy near the transition — a signature of the Cantor-set spectral structure of quasiperiodic operators [20] — but becomes clearly and persistently positive above $\eta_i^* \approx 2.2$ for the aperiodic case, and $\eta_i^* \approx 3.0$ for the periodic case, a factor of approximately $1.4\times$ lower threshold in the aperiodic case. The localisation length $\xi = 1/\gamma$ diverges as $\eta_i \rightarrow \eta_i^*$ from above and decreases for $\eta_i > \eta_i^*$.

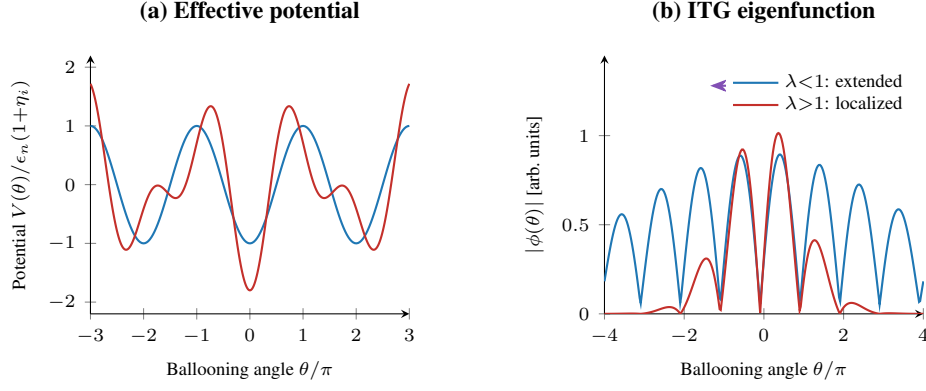


Figure 1. (a) Effective potential $V(\theta)$: the periodic potential $(-\cos\theta)$ (blue) and the aperiodic potential $(-\cos\theta - \lambda \cos(\alpha\theta))$ with $\lambda = 0.8$, $\alpha = 1.618$ (golden ratio) in red. (b) ITG eigenfunction $|\phi(\theta)|$ in ballooning space: extended for $\lambda < 1$ (blue), exponentially localized for $\lambda > 1$ (red) with localisation length $\xi = 1/\ln \lambda$.

It is important to distinguish the AAH localisation from the single-well localisation that arises even in a periodic geometry. In a single bad-curvature well, ITG eigenmodes acquire a Gaussian envelope with localisation parameter $\lambda_{\text{loc}} \sim \sqrt{\omega \bar{\omega}_d} / \omega_i^2$, confining the mode within one connection length [21, 22]. The AAH localisation is qualitatively different: it arises from the incommensurate aperiodicity across *many* field-line periods, with localisation length $\xi = 1/\gamma$. Near marginal stability, single-well localisation weakens ($\lambda_{\text{loc}} \rightarrow 0$ as $\omega \rightarrow 0$ [22]), and it is the global AAH mechanism that determines η_i^* .

The Anderson transition at η_i^* creates a structure directly analogous to the second stability regime in MHD ballooning theory. Below η_i^{lin} , no modes are unstable. Between η_i^{lin} and η_i^* , modes are linearly unstable *and* extended in ballooning space. Above η_i^* , modes remain linearly unstable but are now Anderson-localized: their eigenfunctions are exponentially confined in ballooning space and cannot sustain coherent cross-field perturbations. This is conjectured to be the low-transport second regime. In MHD ballooning theory, the second stability boundary arises from linear restabilization by the Shafranov shift; here it arises from topological localisation of the eigenmodes by the quasiperiodic curvature spectrum. The connection between eigenmode localisation and transport suppression is physically well-motivated — localized eigenfunctions cannot drive coherent cross-field flux — but has not yet been derived rigorously and remains a prediction of the theory, to be tested by simulations and experiment.

3.2. From the Anderson-localized regime to temperature clamping

The Anderson localisation threshold η_i^* marks the entry into the low-transport second regime, but does not by itself determine exactly where the gradient settles within that regime. The observed gradient $\eta_i^{\text{obs}} \gtrsim \eta_i^*$ is set by the balance between heating and whatever residual transport (nonlinear or kinetic) survives in the Anderson-localized phase — a balance that our fluid model does not calculate. What the Anderson mechanism does determine, however, is that the *boundary* η_i^* of this regime

is power-independent: it depends only on equilibrium geometry (λ , α , ϵ_n) and not on P_{heat} . Since the observed gradient cannot fall below η_i^* without leaving the low-transport phase and encountering the extended modes that drive transport, the gradient is bounded below by a power-independent geometric quantity. This is the sense in which Anderson localisation explains temperature clamping: it enforces a power-independent lower bound on η_i^{obs} , and if the residual transport in the localized phase is weak enough that η_i^{obs} is not pushed far above η_i^* , the gradient — and through it T_i^* — will be approximately power-independent.

The connection to temperature clamping follows from the exponential profile relation. With $L_{T_i} \approx L_n / \eta_i^{\text{obs}}$ throughout the confinement region, the central ion temperature satisfies

$$T_i^*(0) \approx T_i(a) \exp\left(\frac{a \eta_i^{\text{obs}}}{L_n}\right), \quad (12)$$

where $T_i(a)$ is the edge temperature set by scrape-off layer physics. The ratio $\tau^* = T_e / T_i^*$ is then

$$\tau^* \approx \frac{T_e}{T_i(a)} \exp\left(-\frac{a \eta_i^{\text{obs}}}{L_n}\right). \quad (13)$$

To the extent that $\eta_i^{\text{obs}} \approx \eta_i^*$ (i.e. that the gradient does not penetrate far into the localized phase), τ^* is determined by geometric quantities alone and is independent of P_{heat} .

Three further qualitative predictions follow from the present model. *First*, η_i^* increases as λ decreases. *Second*, η_i^* increases as ϵ_n decreases: a flatter density profile deepens the effective potential more slowly, requiring higher η_i to enter the localized phase. *Third*, deliberately changing λ — for instance by modifying the aperiodic harmonic content of the equilibrium field — should enable one to control η_i^* in a predictable, geometry-dependent way. The quantitative implementation of such a perturbation in stellarator reactor design and experiments is left for future work.

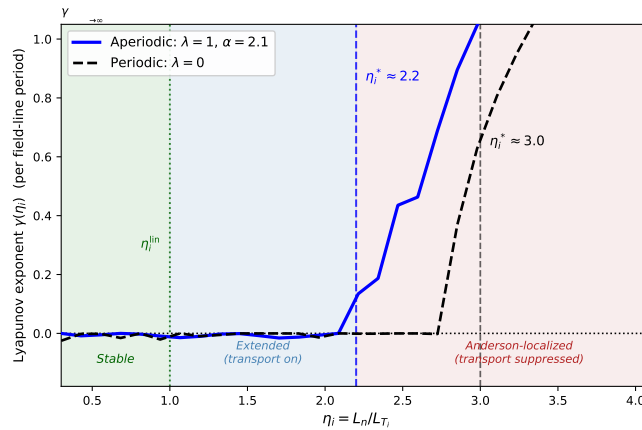


Figure 2. Three-threshold structure. Lyapunov exponent $\gamma(\eta_i)$ per field-line period evaluated at $\Lambda = 0$ as a function of the ion temperature gradient η_i . The aperiodic model uses with $\lambda = 1$, $\alpha = 2 + \sqrt{2}/10 \simeq 2.14$, and $\epsilon_n = 0.12$. The legend displays this as $\alpha \simeq 2.1$. The periodic comparison has $\lambda = 0$ with the same ϵ_n . The Lyapunov exponent becomes persistently positive at $\eta_i^* \simeq 2.2$ for the aperiodic case and at $\eta_i^* \simeq 3.0$ for the periodic comparison. For the periodic case, $\gamma > 0$ indicates an ordinary Floquet gap rather than Anderson localization. The blue shaded region is the extended mode-structure regime; the red shaded region is the localized mode-structure regime, where transport suppression is conjectured but requires nonlinear verification.

4. Discussion

The argument presented here is deliberately minimal. The AAH mapping identifies a structural property of the ITG eigenvalue problem in aperiodic geometry — the existence of a sharp localisation transition — and connects it qualitatively to the observed gradient clamping.

Several limitations should be stated clearly. *First*, the connection between AAH localisation in ballooning space and suppression of cross-field transport is physical and well-motivated but not yet derived rigorously. The claim is that extended ballooning eigenmodes sustain coherent perturbations across flux surfaces and drive transport, while localized eigenmodes do not. A quantitative derivation of this connection is the natural next step and will be reported separately. *Second*, the present model is applicable in a fluid, long-wavelength regime. Electromagnetic effects, trapped electrons, and finite Larmor radius corrections will modify the coefficients in the fluid equations. The kinetic framework (for instance, [22]) provides the appropriate description of single-well localisation with these effects retained; incorporating their kinetic dispersion function into the global aperiodic eigenvalue problem is the natural next step. *Third*, the AAH exact results ($\gamma = \ln \lambda_{\text{AAH}}$, transition at $\lambda_{\text{AAH}} = 1$) apply to the *discrete* tight-binding model with effective coupling λ_{AAH} (Appendix B), not to the geometric ratio λ directly. The present equation is a *continuous* quasiperiodic Hill equation, for which the localisation transition is generic but the precise threshold is sensitive to the precise magnetic geometry.

The present work complements a parallel line of research on Anderson localisation of MHD ballooning modes in non-axisymmetric geometry [10, 11, 12]. Bhattacharjee [12] shows that geometric aperiodicity localizes MHD pressure-driven eigenmodes and formulates the resulting nonlinear stability as

a connectivity phase transition on a Ginzburg–Landau network. The present paper identifies the same aperiodicity-driven localisation for ITG eigenmodes, with the additional consequence of a low-transport second regime above η_i^* — the ITG analogue of the MHD second stability boundary. The two mechanisms are independent — MHD ballooning stability and ITG transport operate on different timescales and involve different mode types — but both arise from the same underlying structure: aperiodic coefficients in the ballooning equation producing Anderson-localized eigenmodes.

5. Conclusion

We have established the following:

1. The ITG eigenvalue equation in aperiodic stellarator geometry is a quasiperiodic Hill equation whose structure maps onto the Aubry–André–Harper model in the limit of a single dominant incommensurate curvature harmonic and long perpendicular wavelength. The reduction to a quasiperiodic Hill equation is rigorous within the fluid closure. The further reduction to an AAH difference equation is a controlled tight-binding approximation.
2. For the reduced continuous Hill equation, the relevant localisation diagnostic is the Lyapunov exponent. In the illustrative two-harmonic model, the Lyapunov exponent at the drift-wave-resonant value $\Lambda = 0$ becomes positive above a geometry-dependent threshold η_i^* . This is the continuous-equation analogue of the sharp AAH transition in the tight-binding limit. In a periodic device (tokamak) no such transition exists.
3. For the model two-harmonic curvature profile $K(\theta) = \cos \theta + \lambda \cos(\alpha \theta)$ with $\lambda = 1$, $\alpha = 2.1$, $\epsilon_n = 0.12$, the Lyapunov exponent gives the gradient threshold $\eta_i^* \simeq$

2.0. The accurate threshold for any real device requires computing the Lyapunov exponent from the full Boozer harmonic spectrum of the equilibrium state for the device, which is sensitive to geometry.

4. Above η_i^* , the reduced eigenmode problem enters a regime with positive Lyapunov exponent and exponentially localized field-line structure. We conjecture that this localisation suppresses coherent cross-field heat transport, thereby producing a low-transport second regime. The transport consequence requires nonlinear gyrokinetic verification. If verified, this creates a low-transport second regime above the linear instability threshold, the ITG analogue of the second stability regime in MHD ballooning theory.

Appendix A: From the fluid ITG ballooning equation to the quasiperiodic Hill model

We derive the reduced drift-wave-resonant ITG equation used in the main text. The purpose of the derivation is not to compute the full kinetic ITG growth rate, but to obtain the leading-order mode-structure equation along a field line. The calculation follows the spirit of the straight-stellarator fluid model of Bhattacharjee et al., but we write the magnetic-drift drive in a form suitable for general stellarator geometry.

Let s denote distance along a field line, x the radial coordinate, and y the binormal coordinate. We consider perturbations of the form

$$\delta f = \tilde{f}(s) \exp(ik_y y - i\omega t).$$

The equilibrium density and ion temperature satisfy

$$\frac{d \ln n_0}{dx} = -\frac{1}{L_n}, \quad \frac{d \ln T_{i0}}{dx} = -\frac{1}{L_{T_i}}, \quad \eta_i \equiv \frac{L_n}{L_{T_i}}.$$

We define

$$\varphi \equiv \frac{e\delta\Phi}{T_e}, \quad N \equiv \frac{\delta n_i}{n_0}, \quad \Theta \equiv \frac{\delta T_i}{T_i},$$

and

$$\omega_* \equiv \omega_{*e} = \frac{k_y c T_e}{e B L_n}.$$

The field-line-dependent magnetic-drift frequency is denoted $\omega_d(s)$. We define the dimensionless drift function

$$\epsilon_d(s) \equiv \frac{\omega_d(s)}{\omega_*}.$$

In a simple large-aspect-ratio circular tokamak model, $\epsilon_d \simeq 2(L_n/R) \cos \theta$, up to sign convention. In a stellarator, however, $\omega_d(s)$ should be computed from the actual curvature and grad- B drift projected onto the binormal wavevector.

For adiabatic electrons,

$$\frac{\delta n_e}{n_0} = \frac{e\delta\Phi}{T_e} = \varphi. \quad (14)$$

In the long-wavelength limit $k_\perp^2 \rho_s^2 \ll 1$, quasineutrality then gives

$$N = \varphi. \quad (15)$$

The ion temperature perturbation is produced by $E \times B$ advection of the equilibrium ion-temperature gradient:

$$\frac{\partial \Theta}{\partial t} + \mathbf{v}_E \cdot \nabla \ln T_i = 0. \quad (16)$$

Since

$$v_{Ex} = -\frac{c}{B} \frac{\partial \delta\Phi}{\partial y} = -ik_y \frac{c}{B} \delta\Phi,$$

we obtain

$$-i\omega\Theta + i\eta_i\omega_*\varphi = 0,$$

or

$$\Theta = \frac{\eta_i\omega_*}{\omega}\varphi.$$

The linearized ion continuity equation is

$$-i\omega N + i\omega_*\varphi + \frac{\partial u_\parallel}{\partial s} - i\omega_d(s)(N + \Theta) = 0. \quad (17)$$

The sign convention has been chosen such that positive ω_d corresponds to bad curvature and gives the destabilizing sign in the final Hill equation. Using $N = \varphi$, this becomes

$$-i(\omega - \omega_*)\varphi + \frac{\partial u_\parallel}{\partial s} - i\omega_d(s) \left(1 + \frac{\eta_i\omega_*}{\omega}\right) \varphi = 0.$$

The minimal parallel ion momentum equation is

$$-i\omega u_\parallel = -c_s^2 \frac{\partial \varphi}{\partial s}, \quad c_s^2 = \frac{T_e}{m_i}.$$

Thus

$$\frac{\partial u_\parallel}{\partial s} = -i \frac{c_s^2}{\omega} \frac{\partial^2 \varphi}{\partial s^2}.$$

Substitution gives

$$-i(\omega - \omega_*)\varphi - i \frac{c_s^2}{\omega} \frac{\partial^2 \varphi}{\partial s^2} - i\omega_d(s) \left(1 + \frac{\eta_i\omega_*}{\omega}\right) \varphi = 0.$$

Multiplying by $i\omega$, we obtain the fluid equation

$$c_s^2 \frac{\partial^2 \varphi}{\partial s^2} + [\omega(\omega - \omega_*) + \omega_d(s)(\omega + \eta_i\omega_*)] \varphi = 0. \quad (18)$$

Now introduce

$$\theta = \frac{\omega_*}{c_s} s, \quad \Omega = \frac{\omega}{\omega_*}, \quad \epsilon_d(\theta) = \frac{\omega_d(s)}{\omega_*}.$$

The dimensionless equation is

$$\frac{d^2 \varphi}{d\theta^2} + [\Omega(\Omega - 1) + \epsilon_d(\theta)(\Omega + \eta_i)] \varphi = 0.$$

If we write $\epsilon_d(\theta) = \epsilon_n K(\theta)$, this becomes

$$\frac{d^2 \varphi}{d\theta^2} + [\Omega(\Omega - 1) + \epsilon_n K(\theta)(\Omega + \eta_i)] \varphi = 0.$$

This is equation (1), our point of departure in the main text.

Appendix B: From the continuous Hill equation to the tight-binding AAH model

We derive the explicit form of the hopping amplitude t and on-site modulation V that connect the continuous quasiperiodic Hill equation (3) to the discrete Aubry–André–Harper tight-binding model, via Wannier function projection onto the lowest Mathieu band.

We set $\lambda = 0$ and write Eq. (3) in Schrödinger form:

$$\hat{H}_0 \psi \equiv \left(-\frac{d^2}{d\theta^2} - A \cos \theta \right) \psi = E \psi, \quad A = \epsilon_n(1 + \eta_i). \quad (19)$$

with $A = \epsilon_n(1 + \eta_i)$. This is the Mathieu equation, whose solutions are Bloch functions $\psi_k(\theta) = e^{ik\theta} u_k(\theta)$ with u_k periodic and band energies $E_0(k)$ for the lowest band.

The Wannier function for the lowest band centred on site m (field-line period $2\pi m$) is

$$w_m(\theta) = w_0(\theta - 2\pi m) = \frac{1}{2\pi} \int_0^1 e^{-2\pi i k m} \psi_k(\theta) dk, \quad (20)$$

where the integral runs over the first Brillouin zone $k \in [0, 1)$. These are exponentially localised around each curvature well and satisfy $\langle w_m | w_{m'} \rangle = \delta_{mm'}$.

Projecting \hat{H}_0 onto the Wannier basis gives the tight-binding matrix elements. The nearest-neighbour hopping amplitude is

$$t \equiv -\langle w_0 | \hat{H}_0 | w_1 \rangle = -\int_{-\infty}^{\infty} w_0(\theta) \hat{H}_0 w_0(\theta - 2\pi) d\theta. \quad (21)$$

Since \hat{H}_0 is diagonal in the Bloch basis with eigenvalue $E_0(k)$, the Wannier matrix element (21) is the first Fourier coefficient of $E_0(k)$:

$$t = -\int_0^1 E_0(k) e^{2\pi i k} dk \approx \frac{E_0(k=0) - E_0(k=\frac{1}{2})}{4}, \quad (22)$$

where the approximation retains only the fundamental harmonic of $E_0(k)$ (justified when higher harmonics t_2, t_3, \dots are exponentially small in A). Equation (22) identifies t as one quarter of the lowest Mathieu band's full width, $t = \frac{1}{4} W(A)$, with $W = E_0(0) - E_0(\frac{1}{2}) > 0$ (the band is narrowest at large A when modes are tightly confined in each well).

The quasiperiodic part $A\lambda \cos(\alpha\theta)$ gives diagonal matrix elements

$$V_m \equiv A\lambda \langle w_m | \cos(\alpha\theta) | w_m \rangle = A\lambda \mathcal{F}_\alpha \cos(2\pi\alpha m + \delta), \quad (23)$$

where the form factor

$$\mathcal{F}_\alpha \equiv \int_{-\infty}^{\infty} |w_0(\theta)|^2 \cos(\alpha\theta) d\theta \quad (24)$$

is the cosine transform of the Wannier probability density at the quasiperiodic wavenumber α . For small A , $w_0(\theta)$ is approximately a Gaussian of width $\sigma \sim (A/2)^{-1/4}$, giving $\mathcal{F}_\alpha \approx \exp(-\alpha^2 \sigma^2 / 2)$; for larger A the exact value must be computed numerically from the Mathieu eigenfunctions.

Off-diagonal matrix elements $\langle w_m | \cos(\alpha\theta) | w_{m'} \rangle$ with $m \neq m'$ are suppressed by the exponential localisation of the Wannier functions and are neglected in the single-band approximation.

Expanding $\phi(\theta) = \sum_m c_m w_0(\theta - 2\pi m)$ and retaining only nearest-neighbour hopping, the eigenvalue problem reduces to

$$-t(c_{m+1} + c_{m-1}) + A\lambda \mathcal{F}_\alpha \cos(2\pi\alpha m + \delta) c_m = (E - E_0) c_m, \quad (25)$$

which is the standard Aubry–André–Harper equation [8] with coupling constant

$$\lambda_{\text{AAH}} = \frac{A\lambda \mathcal{F}_\alpha}{2|t|} = \frac{\epsilon_n(1 + \eta_i)\lambda \mathcal{F}_\alpha}{2|t|}. \quad (26)$$

The Aubry–André transition occurs at

$$|\lambda_{\text{AAH}}| = 1, \quad \text{or equivalently} \quad A\lambda \mathcal{F}_\alpha = 2|t|. \quad (27)$$

The Aubry–André exact result gives localisation for $\lambda_{\text{AAH}} > 1$, which is a transcendental condition on $A = \epsilon_n(1 + \eta_i)$ that determines the single-band estimate of the threshold η_i^* . Note that $W(A) = E_0(k=0) - E_0(k=\frac{1}{2})$ can be negative (the ground-state band energy is *lower* at $k=0$ than at $k=\frac{1}{2}$ for the physical operator $\hat{H}_{\text{phys}} = -d^2/d\theta^2 - A \cos \theta$); the localisation condition uses $|\lambda_{\text{AAH}}|$ and is independent of this sign convention. The exact threshold for the *continuous* equation — used throughout the main text — is given instead by the Mathieu Lyapunov condition $\gamma(\eta_i^*) = 0$ (Section 3.1), which automatically includes inter-band coupling and higher-order hoppings. A quantitative comparison of the discrete ($\lambda_{\text{AAH}} = 1$) and continuous ($\gamma = 0$) thresholds requires computing $W(A)$ and $\mathcal{F}_\alpha(A)$ from the actual Mathieu eigenfunctions, which we leave to future work.

Acknowledgements

We would like to thank Per Helander and Hongxuan Zhu for enlightening discussions. We acknowledge the use of ChatGPT, Claude (Anthropic), and Gemini for writing assistance, crafting illustrations, and literature search.

Competing Interests

We declare no competing interests.

Data Availability

No new experimental data were generated.

References

- [1] C. D. Beidler, H. M. Smith, A. Alonso, T. Andreeva, J. Baldzuhn, M. N. A. Beurskens, M. Borchardt, S. A. Bozhnikov, K. J. Brunner, H. Damm, M. Drevlak, O. P. Ford, G. Fuchert, J. Geiger, P. Helander, U. Hergenbahn, M. Hirsch, U. Höfel, Ye. O. Kazakov, R. Kleiber, M. Krychowiak, S. Kwak, A. Langenberg, H. P. Laqua, U. Neuner, N. A. Pablant, E. Pasch, A. Pavone, T. S. Pedersen, K. Rahbarnia, J. Schilling, E. R. Scott, T. Stange, J. Svensson, H. Thomsen, Y. Turkin, F. Warmer, R. C. Wolf, D. Zhang and the W7-X Team, Demonstration of reduced neoclassical energy transport in Wendelstein 7-X. *Nature* **596**, 221–226 (2021).
- [2] M. N. A. Beurskens, S. A. Bozhnikov, O. Ford, P. Xanthopoulos, A. Zocco, Y. Turkin, A. Alonso, C. Beidler, I. Calvo, D. Carralero, T. Estrada, G. Fuchert, O. Grulke, M. Hirsch, K. Ida, M. Jakubowski, C. Killer, M. Krychowiak, S. Kwak, S. Lazerson, A. Langenberg, R. Lunsford, N. Pablant, E. Pasch, A. Pavone, F. Reimold, Th. Romba, A. von Stechow, H. M. Smith, T. Windisch, M. Yoshinuma, D. Zhang, R. C. Wolf and the W7-X Team, Ion temperature clamping in Wendelstein-7X electron cyclotron heated plasmas. *Nucl. Fusion* **61**, 116072 (2021).
- [3] K. Nagaoka, H. Takahashi, S. Murakami, H. Nakano, Y. Takeiri, H. Tsuchiya, M. Osakabe, K. Ida, M. Yokoyama, M. Yoshinuma, S. Morita, M. Goto, T. Oishi, N. Pablant, K. Fujii, K. Tanaka, N. Tamura, Y. Nakamura, X. Du, T. Ido, A. Shimizu, S. Kubo, H. Igami, R. Seki, C. Suzuki, Y. Suzuki, K. Tsumori, K. Ikeda, M. Kisaki, Y. Yoshimura, T. Shimozuma, T. Seki, K. Saito, H. Kasahara, S. Kamio, T. Mutoh, O. Kaneko, H. Yamada, A. Komori and the LHD Experiment Group, Ion thermal transport and ion temperature clamping in LHD. *Nucl. Fusion* **55**, 113020 (2015).
- [4] F. Romanelli, Ion temperature-gradient-driven modes and anomalous ion transport. *Phys. Fluids B* **1**, 1018 (1989).
- [5] F. Romanelli and F. Zonca, The radial structure of the ion-temperature-gradient-driven mode. *Phys. Fluids B* **5**, 4081 (1993).
- [6] K. Ida and T. Fujita, Internal transport barrier in tokamak and helical plasmas. *Plasma Phys. Control. Fusion* **60**, 033001 (2018).
- [7] P. W. Anderson, Absence of diffusion in certain random lattices. *Phys. Rev.* **109**, 1492 (1958).
- [8] S. Aubry and G. André, Analyticity breaking and Anderson localisation in incommensurate lattices. *Ann. Israel Phys. Soc.* **3**, 133 (1980).
- [9] P. G. Harper, Single band motion of conduction electrons in a uniform magnetic field. *Proc. Phys. Soc. A* **68**, 874 (1955).
- [10] P. Cuthbert and R. L. Dewar, Anderson-localized ballooning modes in general toroidal plasmas. *Phys. Plasmas* **7**, 2302 (2000).
- [11] M. H. Redi, J. L. Johnson, S. Klasky, J. Canik, R. L. Dewar and W. A. Cooper, Anderson localisation of ballooning modes, quantum chaos and the stability of compact quasiaxially symmetric stellarators. *Phys. Plasmas* **9**, 1990 (2002).
- [12] A. Bhattacharjee, Topological arrest of ballooning modes in non-axisymmetric plasmas. Preprint arXiv:2602.07329 (2026).
- [13] J. W. Connor, R. J. Hastie and J. B. Taylor, Shear, periodicity, and plasma ballooning modes. *Phys. Rev. Lett.* **40**, 396 (1978).
- [14] A. Bhattacharjee, J. E. Sedlak, P. L. Similon, M. N. Rosenbluth and D. W. Ross, Drift waves in a straight stellarator. *Phys. Fluids* **26**, 880 (1983).
- [15] L. Podavini, A. Zocco, J. M. García-Regaña, M. Barnes, F. I. Parra, A. Mishchenko and P. Helander, Ion-temperature- and density-gradient-driven instabilities and turbulence in Wendelstein 7-X close to the stability threshold. *J. Plasma Phys.* **90**, 905900414 (2024).
- [16] H. Thienpondt, J. M. García-Regaña, I. Calvo, G. Acton and M. Barnes, Influence of the density gradient on turbulent heat transport at ion-scales: an inter-machine study with the gyrokinetic code stella. *Nucl. Fusion* **65**, 016062 (2025).
- [17] V. I. Arnold, *Mathematical Methods of Classical Mechanics*, 2nd edn. Springer (1989), Appendix 8.
- [18] G. Benettin, L. Galgani, A. Giorgilli and J.-M. Strelcyn, Lyapunov characteristic exponents for smooth dynamical systems and for Hamiltonian systems; a method for computing all of them. *Meccanica* **15**, 9–30 (1980).
- [19] V. I. Oseledets, A multiplicative ergodic theorem: Lyapunov characteristic numbers for dynamical systems. *Trans. Moscow Math. Soc.* **19**, 197–231 (1968).
- [20] J. E. Avron and B. Simon, Almost periodic Schrödinger operators II: the integrated density of states. *Duke Math. J.* **50**, 369–391 (1983).
- [21] T. S. Hahm and W. M. Tang, Properties of ion temperature gradient drift instabilities in H-mode plasmas. *Phys. Fluids B* **1**, 1185 (1989).
- [22] E. Rodríguez and A. Zocco, The kinetic ion-temperature-gradient-driven instability and its localisation. *J. Plasma Phys.* **91**, E21 (2025).